The Journal of Immunology

ARTD1 in Myeloid Cells Controls the IL-12/18–IFN-γ Axis in a Model of Sterile Sepsis, Chronic Bacterial Infection, and Cancer

Friedrich A. Kunze, Michael Bauer, Juliana Komuczki, Margit Lanzinger, Kapila Gunasekera, Ann-Katrin Hopp, Mareike Lehmann, Burkhard Becher, Anne Müller and Michael O. Hottiger

J Immunol 2019; 202:1406-1416; Prepublished online 23 January 2019;
doi: 10.4049/jimmunol.1801107
http://www.jimmunol.org/content/202/5/1406

The Journal of Immunology is published twice each month by
The American Association of Immunologists, Inc.,
1451 Rockville Pike, Suite 650, Rockville, MD 20852

Print ISSN: 0022-1767 Online ISSN: 1550-6606.

ARTD1 in Myeloid Cells Controls the IL-12/18–IFN-γ Axis in a Model of Sterile Sepsis, Chronic Bacterial Infection, and Cancer

Friedrich A. Kunze,[*,†] Michael Bauer,[‡,§] Juliana Komuczki,[†,¶] Margit Lanzinger,[†,¶] Kapila Gunasekera,[*] Ann-Katrin Hopp,[*,†] Mareike Lehmann,[*,‖] Burkhard Becher,[¶] Anne Müller,[‡] and Michael O. Hottiger[*]

Mice deficient for ADP-ribosyltransferase diphteria toxin–like 1 (ARTD1) are protected against microbially induced inflammation. To address the contribution of ARTD1 to inflammation specifically in myeloid cells, we generated an *Artd1*$^{\Delta Myel}$ mouse strain with conditional ARTD1 deficiency in myeloid lineages and examined the strain in three disease models. We found that ARTD1, but not its enzymatic activity, enhanced the transcriptional activation of distinct LPS-induced genes that included IL-12, TNF-α, and IL-6 in primary bone marrow–derived macrophages and LPS-induced IL-12/18–IFN-γ signaling in *Artd1*$^{\Delta Myel}$ mice. The loss of *Artd1* in myeloid cells also reduced the T_H1 response to *Helicobacter pylori* and impaired immune control of the bacteria. Furthermore, *Artd1*$^{\Delta Myel}$ mice failed to control tumor growth in a s.c. MC-38 model of colon cancer, which could be attributed to reduced T_H1 and CD8 responses. Together, these data provide strong evidence for a cell-intrinsic role of ARTD1 in myeloid cells that is independent of its enzymatic activity and promotes type I immunity by promoting IL-12/18 expression. *The Journal of Immunology*, 2019, 202: 1406–1416.

Inflammation is orchestrated by various cell types that integrate diverse stimuli for the generation of a specific immune response to kill invading pathogens and/or regenerate damaged tissue (1). Pathogen recognition receptors initiate innate immune responses and are expressed on macrophages and dendritic cells but also epithelial and endothelial cells and fibroblasts (2). Pathogen recognition receptors recognize conserved pathogen-associated molecular patterns, such as bacterial and fungal cell wall components (e.g., LPS) or danger-associated molecular patterns (1). The recognition of pathogen-associated molecular patterns and danger-associated molecular patterns, often by the same receptors, activates intracellular signaling pathways, which results in the expression of proinflammatory cytokines such as IL-12, IL-23, IL-6, and IL-1β (3). IL-12, produced by APCs in response to microbial infection, activates NK, $CD4^+$, and $CD8^+$ T cells and promotes T_H1 differentiation and IFN-γ production (1).

Septic shock is the most common cause of death in intensive care units and is usually the result of a systemic Gram-negative bacterial infection resulting in hypotension and failure of vital organs, in particular the liver, kidney, and heart (4). The bacterial membrane component LPS, when injected into animals, causes a shock-like state that can lead to death. Mechanistically, LPS activates the NF-κB/Rel family of transcription factors, which transactivate critical genes involved in the pathogenesis of septic shock mediated by excessive T_H1/T_H17 immune responses (5). LPS binding to TLR4 induces the activation of several primary response genes, such as *Ifnb1* and *Ccl5* (6). We and others have reported that ADP-ribosyltransferase diphteria toxin–like 1 (ARTD1) promotes the NF-κB–dependent expression of proinflammatory cytokines such as IL-1β, IL-6, TNF-α, and CXCL-2 and of adhesion molecules such as ICAM, VCAM, or E-selectin in LPS- or TNF-α–stimulated macrophages and fibroblasts (7–9). ARTD1 belongs to the family of intracellular diphtheria toxin–like ADP-ribosyltransferases that covalently attach ADP-ribose to amino acid residues of target proteins using NAD^+ as substrate. This process is called protein ADP-ribosylation and represents an ancient posttranslational modification found in a wide range of species (10). Protein ADP-ribosylation can either affect the enzymatic activity of the modified protein or the interaction with

*Department of Molecular Mechanisms of Disease, University of Zurich, 8057 Zurich, Switzerland; †Molecular Life Science Ph.D. Program of the Life Science Zurich Graduate School, 8057 Zurich, Switzerland; ‡Institute of Molecular Cancer Research, University of Zurich, 8057 Zurich, Switzerland; §Cancer Biology Ph.D. Program of the Life Science Zurich Graduate School, 8057 Zurich, Switzerland; ¶Institute of Experimental Immunology, University of Zurich, 8057 Zurich, Switzerland; and ‖Comprehensive Pneumology Center, Ludwig Maximilian University, University Hospital Grosshadern, and Helmholtz Center Munich, 81377 Munich, Germany

ORCIDs: 0000-0002-2518-3320 (M.B.); 0000-0002-2570-531X (K.G.); 0000-0002-8601-8206 (M. Lehmann); 0000-0002-7323-2270 (M.O.H.).

Received for publication August 8, 2018. Accepted for publication December 19, 2018.

This work was supported by Swiss National Science Foundation Grant BSCGIO_157841/1 to the laboratory of A.M. ADP-ribosylation research in the laboratory of M.O.H. was funded by the Canton of Zurich and Swiss National Science Foundation Grant 310030_157019.

F.A.K. generated the mice and performed the LPS in vivo models, RNA sequencing, ELISA, quantitative PCR, and Western blot analyses. J.K. and M. Lanzinger performed intracellular cytokine staining and immunophenotyping of the LPS models. M.B. performed the *Helicobacter pylori* and MC-38 studies. K.G. analyzed the RNA sequencing. A.-K.H. assisted with the LPS experiments. M. Lehmann helped in generating the floxed ARTD1 mouse. F.A.K. and M.O.H. prepared the manuscript. M.O.H., A.M., and B.B. directed and supervised all aspects of the study. All authors critically reviewed the manuscript.

The sequences presented in this article have been submitted to the National Center for Biotechnology Information (https://www.ncbi.nlm.nih.gov/bioproject/506145) under accession number PRJNA506145.

Address correspondence and reprint requests to Prof. Michael O. Hottiger, University of Zurich, Winterthurerstrasse 190, Zurich 8057, Switzerland. E-mail address: michael.hottiger@dmmd.uzh.ch

The online version of this article contains supplemental material.

Abbreviations used in this article: ARTD1, ADP-ribosyltransferase diphteria toxin–like 1; BMDM, bone marrow–derived macrophage; ESC, embryonic stem cell; ICS, intracellular cytokine staining; PARPi, PARP inhibitor; qRT-PCR, quantitative RT-PCR.

nucleic acids and with other proteins (11). ARTD1 is best known for its role during the DNA damage response, particularly the base excision repair and double strand break repair pathways (12). The concept that the inhibition of the DNA-repair machinery could sensitize tumor cells to conventional DNA damage–based therapies such as chemo- or radiotherapy has led to the development of small molecule ADP-ribosylation inhibitors (i.e., PARP inhibitors [PARPi]) (13). Today, U.S. Food and Drug Administration–approved PARPi are clinically used to treat breast and ovarian cancer patients. In addition, these compounds have also been reported to dampen various types of inflammation, potentially contributing to their antitumor activity (13). Beneficial effects of PARPi have been reported in numerous inflammatory disease models, confirming that ADP-ribosylation broadly regulates inflammatory processes (14). ARTD1 function during transcriptional gene regulation in various cells types is further supported by the fact that ARTD1 knockout mice are resistant to a high dose of LPS in an endotoxic shock model (15), suggesting a dominant role of ARTD1 during inflammatory signaling. However, it is not clear which cell type or types are contributing to this phenotype.

We have shown previously that the PARPi PJ34 prevents and cures *Helicobacter pylori*–associated, T cell–driven immunopathology that precedes gastric cancer development. *H. pylori* causes a persistent mucosa-associated but non-invasive infection that is characterized by either regulatory T cell or T_H1/T_H17 immune responses (16). *H. pylori*–infected mice exhibit a striking effector T cell infiltrate that limits the bacterial burden without clearing *H. pylori* completely (17, 18). Rather, the large quantities of IFN-γ produced by *H. pylori*–specific T_H1 cells are believed to directly cause premalignant lesions (i.e., epithelial hyperplasia and intestinal metaplasia that precede the development of gastric cancer) (17). PJ34 exerts its anti-inflammatory effects by impairing T cell priming and T_H1 polarization in the gut-draining mesenteric lymph nodes (19). Our data indicated that PJ34 directly suppresses T cell effector functions by blocking the IFN-γ production of mesenteric lymph node T cells. However, it was not clear whether ARTD1 or another ARTD family member contributed to these observations and to what extent ARTD1 regulates a specific cell type that contributed to the T_H1 polarization. ARTD1's nuclear localization in LPS-stimulated macrophages hinted at its possible role in mediating certain nuclear effects elicited by LPS, a possibility also suggested by previous reports describing a transcriptional coregulator activity of ARTD1 (20–22).

Tumors are commonly infiltrated by heterogeneous populations of myeloid cells that are of monocytic and granulocytic origin and have considerable phenotypic plasticity with both positive and negative effects on tumor growth and metastasis (23, 24). The balance between antitumor and protumor functions can depend on the polarization state, the interaction with the tumor microenvironment, and/or the tumor type (25). Syngeneic, s.c. growing MC-38 mouse colon adenocarcinoma cells have been used extensively to study the role of macrophages in antitumor immunity (26). We have reported recently that MC-38 cells express functional hypoxic (HIF-1α) and inflammatory (p65/RelA) signaling pathways (27). In contrast to myeloid cells, HIF-1α levels remained unaffected in MC-38 cells treated with LPS, and hypoxia failed to induce NF-κB. The corresponding regulation of canonical HIF and NF-κB target genes confirmed these results (27). To what extent ARTD1 in the stroma contributes to the observed effects remains to be uncovered in this model.

To address the role of ARTD1 in myeloid cells during inflammatory and anticancer immune responses, we generated C57BL/6 mice with a Cre-mediated deletion of *Artd1* specifically in myeloid cells ($Artd1^{\Delta Myel}$). We observed that ARTD1 expression in murine macrophages regulates a specific set of genes in a manner that is independent of its enzymatic activity and that *Artd1* deficiency reduces LPS-induced IL-12/18–IFN-γ signaling in an acute in vivo model of sterile sepsis. Moreover, in the abovementioned bacterial infection model using *H. pylori* as the infectious agent, $Artd1^{\Delta Myel}$ mice exhibited reduced IFN-γ expression in gastric $CD4^+$ T cells and failed to control the bacteria. Finally, MC-38 tumor growth was strongly increased in $Artd1^{\Delta Myel}$ mice relative to their wild-type littermates because of reduced activation of $CD4^+$ and $CD8^+$ T cells. Taken together, we provide evidence that ARTD1 in macrophages controls T_H1 responses through regulation of the IL-12/18–IFN-γ axis and that this activity does not require the ADP-ribosylating function of the protein.

Materials and Methods

Animals and animal experiments

The conditional targeting of the *Artd1* allele in embryonic stem cells (ESCs), as well as the generation of the $Artd1^{flox/flox}$ mice, was performed by Polygene as described (28). Briefly, the vector from the European Conditional Mouse Mutagenesis Program (targeting project 45261) was electroporated in C57BL/6 ESCs and analyzed by PCR (*Artd1* localization forward: 5′-CACTGAACTGTCTCCTTAGCCAACTCTGC-3′, reverse: 5′-GGAACTTCGGAATAGGAACTTCGGTTCC-3′; *Artd1* localization forward: 5′-CTAGGATTCTGTGTCTTGACCATGCACTTG-3′, reverse: 5′-CGTATAGCATACATTATACGAAGTTATGTCGAG-3′). Correctly integrated ESC clones were injected into blastocysts, resulting in chimeric mice. Subsequent mating of the chimeric mice with the Flp deleter mice resulted in the Flp-mediated deletion of the gene trap cassette, leaving only the loxP flanked exon 4 of *Artd1* (genotyping primer forward: 5′-GCTTCTACTACCTCCCAAGAAAGAGCG-3′, reverse: 5′-GGCTTTAGTGTGGCAACTTATCCC-3′). To generate whole-body *Artd1* knockout mice ($Artd1^{del/del}$), the generated $Artd^{flox/flox}$ mouse strain was crossed to the CMV-Cre deleter strain (provided by R. Santoro; genotyping primer deleted *Artd1* forward: 5′-GCTTCTACTACCTCCCAAGAAAGAGCG-3′, reverse: 5′-CCTCTGCTGCGTGACTAAGGC-3′). Myeloid-specific *Artd1* knockout mice ($Artd1^{\Delta Myel}$) were generated by crossing $Artd1^{flox/flox}$ mice to *LyzM*-Cre (strain 004781; The Jackson Laboratory) mice. For all experiments, 6–12-wk-old age- and sex-matched mice were used. The sex ratio (male/female) among the animals used in the experiments was 1.01. LPS (*Escherichia coli* O111:B4; Sigma-Aldrich) was injected i.p. at a concentration of 4 mg/kg body weight.

H. pylori infections were performed as described (29). Briefly, mice were infected orally on two consecutive days with 10^8 CFUs of *H. pylori* PMSS1 and analyzed at 1 mo postinfection. The s.c. MC-38 tumor model was performed as described earlier (30). Briefly, colon adenocarcinoma cells (MC-38, 0.5×10^6 cells in 100 μl of PBS) were injected s.c. into both flanks, and tumor progression was determined by caliper measurements every second day. After 2 wk, mice were sacrificed, tumors were weighed, and the volume was calculated using the formula $(a^2 \times b)/2$, where a constitutes the shorter and b the longer dimension of the tumor.

All animals were housed under pathogen-free conditions at the University of Zurich. All animal experiments were carried out in accordance with the Swiss and European Union ethical guidelines and have been approved by the local animal experimentation committee of the Canton Zurich under licenses 207/2015, 266/2014, and ZH140/2017.

Cell culture and reagents

Murine bone marrow–derived macrophages (BMDMs) were generated as previously described (31) and maintained in RPMI 1640 supplemented with 10% FCS, 5% penicillin/streptomycin, and 20 ng/ml recombinant murine M-CSF (PreproTech). Thioglycolate (Sigma-Aldrich)-elicited murine peritoneal macrophages were isolated as described (32). Cell-culture grade LPS (*E. coli* O111:B4) was purchased from Sigma-Aldrich and recombinant murine IFN-γ from PreproTech. The PARPi PJ34 and olaparib were purchased from Selleckchem. MC-38 cells were cultured as described (30).

Multiplex bead array and ELISA

Whole blood serum of mice and cell culture supernatant of BMDMs were analyzed by ELISA (R&D Systems) and by ProcartaPlex Immunoassay (Thermo Fisher Scientific) according to the protocol and measured on a Bio-Plex instrument (Bio-Rad).

Flow cytometry

Flow cytometric analyses of spleens, tumors, and stomach tissue were performed as described earlier (29). Briefly, tissues were cut into pieces and digested with 15 mM HEPES, 500 U/ml type IV collagenase (Sigma-Aldrich), and 0.05 mg ml^{-1} DNase I in RPMI 1640 medium with 10% FBS and 100 U ml^{-1} penicillin/streptomycin, shaking at 37°C for 30–60 min. Subsequently, the samples were pushed through a cell strainer (70 μm) using a syringe plunger, and RBC lysis was performed with a hypotonic buffer (ACK buffer; Life Technologies). Intracellular cytokine staining (ICS) was performed as described earlier (29, 33). Briefly, cells were incubated in RPMI 1640 medium with 10% FBS, 100 U ml^{-1} penicillin/streptomycin, and brefeldin A (BD Biosciences), shaking at 37°C for 4 h. In addition, gastric and tumor suspensions were restimulated with PMA (50 ng/ml), ionomycin (500 ng/ml), or an MC-38–specific tumor peptide. Single cell suspensions were stained with the respective Abs and analyzed on an LSRFortessa and FACSymphony (BD Biosciences). Cell sorting was performed analogously but analyzed by a FACSAria III 5L.

RNA sequencing and bioinformatic analysis

For the library preparation, the quality of the isolated RNA was determined with a Qubit (1.0) Fluorometer (Life Technologies) and a Bioanalyzer 2100 (Agilent). Only those samples with a 260 nm/280 nm ratio between 1.8 and 2.1 and a 28S/18S ratio within 1.5 to 2 were further processed. The TruSeq RNA Sample Prep Kit v2 (Illumina) was used in the subsequent steps. Briefly, total RNA samples (100–1000 ng) were poly-A–enriched and then reverse-transcribed into double-stranded cDNA. The cDNA samples were fragmented, end-repaired, and polyadenylated before ligation of TruSeq adapters containing the index for multiplexing. Fragments containing TruSeq adapters on both ends were selectively enriched with PCR. The quality and quantity of the enriched libraries were validated using a Qubit (1.0) Fluorometer and the Caliper LabChip GX (Caliper Life Sciences). The product is a smear with an average fragment size of ∼260 bp. Library DNA concentrations were normalized to 10 nM in Tris-Cl 10 mM, pH 8.5, with 0.1% Tween 20.

Cluster generation and sequencing were performed using the TruSeq PE Cluster Kit HS4000, or the TruSeq SR Cluster Kit HS4000 (Illumina) was used for cluster generation using 2 nM pooled normalized libraries on the cBOT. Single end sequencing at 125 bp was performed on the Illumina HiSeq 4000, using the TruSeq SBS Kit HS4000 (Illumina).

Reads were quality-checked with FastQC. Sequencing adapters were removed with Trimmomatic (34). Subsequently, reads of at least 20 base length and with an overall average phred quality score >10 were aligned to the reference genome and transcriptome of *Mus Musculus* (FASTA and GTF files, respectively, downloaded from Genome Reference Consortium Mouse Build 38) with STAR v2.5.1 (35) with default settings for single-end reads.

Distribution of the reads across genomic isoform expression was quantified using the R package GenomicRanges (36) from Bioconductor Version 3.0. Differentially expressed genes were identified using the R package edgeR (37) from Bioconductor Version 3.0. A gene is marked as differentially expressed if it possesses the following characteristics: 1) at least 10 counts in at least half of the samples in one group, 2) $p \leq 0.05$, and 3) fold change ≥1.5.

RNA sequencing raw data has been deposited in the National Center for Biotechnology Information BioProject under ID 506145 (https://www.ncbi.nlm.nih.gov/bioproject/506145).

RNA extraction and quantitative real-time PCR analysis

RNA isolation and quantitative real-time PCR were performed as described (38). Briefly, RNA extraction was performed with the NucleoSpin RNA II kit (Macherey-Nagel). RNA was quantified with a NanoDrop and reverse-transcribed using the High-Capacity cDNA Reverse Transcription Kit (Applied Biosystems) according to the supplier's protocol. Quantitative real-time PCRs were performed with the SYBR Green KAPA SYBR FAST (Sigma-Aldrich) and a Rotor-Gene Q 2plex HRM system (QIAGEN). The following genes were quantified with the respective primer pairs: *Il12b* (forward: 5′-GAAGTTCAACATCAAGAGCAGTAG-3′, reverse: 5′-AGGGAGAAGTAGGAATGGGG-3′), *Cxcl3* (forward: 5′-ACCCAGACAGAAGTCATAGCC-3′, reverse: 5′-ACACATCCAGACACCGTTGG-3′), *Cd55* (forward: 5′-CGGGCAAGGTCTCTTCTACC-3′, reverse: 5′-CAGTCTCCGCGTACAGTTGG-3′), *Il23a* (forward: 5′-ACCAGCGGGACATATGAATCT-3′, reverse: 5′-AGACCTTGGCGGATCCTTTG-3′), *Itgax* (forward: 5′-GCAGACACTGAGTGATGCCA-3′, reverse: 5′-TCGGAGGTCACCTAGTTGGG-3′), *Socs1* (forward: 5′-CCGCCAGATGAGCCCAC-3′, reverse: 5′-GGTTGCGTGCTACCATCCTA-3′), *Il18* (forward: 5′-ATGCTTTCTGGACTCCTGCC-3′, reverse: 5′-ATTGTTCCTGGGCCAAGAGG-3′), *Il6* (forward: 5′-CCAATTTCCAATGCTCTCCT-3′, reverse: 5′-ACCACAGTGAGGAATGTCCA-3′), *Tnfa* (forward: 5′-GTCGTAGCAAACCACCAAGTGG-3′, reverse: 5′-GAGATAGCAAATCGGCTGACGG-3′), *Ifng* (forward: 5′-CCTTCTTCAGCAACAGCAAGGCGA-3′, reverse: 5′-TGGACCTGTGGGTTGTTGACCTCA-3′). The relative amounts of each mRNA were normalized to *Rps12* (forward: 5′-GAAGCTGCCAAAGCCTTAGA-3′, reverse: 5′-AACTGCAACCAACCACCTTC-3′).

Western blot

Western blotting was performed as described (39). For Western blot analysis, proteins were separated by SDS-PAGE, and bands were visualized using the Odyssey infrared imaging system (LI-COR). Abs used for Western blotting were anti–PARP-1 (1:1000, sc-7150; Santa Cruz Biotechnology) and anti-tubulin (1:10,000, no. T6199; Sigma).

Results

ARTD1 regulates IL-12/IL-18 gene expression in BMDMs in an enzymatically independent manner

Artd1-deficient mice are protected against microbially induced inflammation. However, the relative contribution of ARTD1 deficiency in specific cell types to the overall phenotype is currently not known. Studies with whole-body *Artd1*-deficient mice in which ARTD1 is absent throughout development and in all cell types have often yielded conflicting results, as ARTD1 is expressed in all examined tissues and cell types (40). To avoid these complications while examining the specific role of ARTD1 in inflammation and to address to what extent ARTD1 in myeloid cells regulates inflammation, we developed a mouse line with a conditional ("floxed") exon 4 of *Artd1* (*Artd1*$^{flox/flox}$) (Supplemental Fig. 1A). To verify the capacity for complete inactivation of the recombined floxed *Artd1* allele, we first crossed *Artd1*$^{flox/flox}$ mice with transgenic *CMV-Cre* deleter mice to generate a full-body *Artd1* knockout (*Artd1*$^{flox/flox}$*;CMV-cre*), hereafter called *Artd1*$^{del/del}$ (Supplemental Fig. 1A–C). The whole-body ARTD1-deficient mouse developed normally and was fertile and thus reproduced observations made with the classical *Parp1*$^{-/-}$ mouse (41). Although Western blotting showed complete loss of ARTD1 in the tested organs (Supplemental Fig. 1D), ARTD1 loss did not affect organ weight or organ structure (Supplemental Fig. 1E and data not shown).

As we aimed to investigate the role of ARTD1 in macrophages and other myeloid cells, we first cultured BMDMs from *Artd1*$^{del/del}$ mice and confirmed the genetic deletion of the *Artd1* gene by quantitative RT-PCR (qRT-PCR) (Supplemental Fig. 1F). BMDMs from *Artd1*$^{del/del}$ mice and *Artd1*$^{flox/flox}$ littermate controls were differentiated for 6 d, treated for 4 h with LPS/IFN-γ, and subjected to RNA sequencing. LPS/IFN-γ stimulation induced a robust proinflammatory gene signature of ∼2500 genes (Fig. 1A), which included many NF-κB target genes (e.g., *Ifnb1*, *Ccl5*, and *Cxcl10*), whereas the expression of many basally expressed genes was reduced (∼3000 genes; Supplemental Fig. 1G). Of the LPS-induced genes, 701 genes were found to be strictly dependent on ARTD1 (i.e., induction was reduced in BMDMs from *Artd1*$^{del/del}$ mice), confirming that ARTD1 acts as a transcriptional coactivator of these genes (Fig. 1B, upper panel). Additionally, we observed that ARTD1 depletion also enhanced the expression of 449 genes (Fig. 1B, lower panel). Independent qRT-PCR analyses of a defined set of genes belonging to either up- or downregulated clusters after ARTD1 depletion confirmed the quantitative RNA sequencing analysis (Fig. 1C). Furthermore, gene ontology analyses of the ARTD1-upregulated genes revealed that ARTD1 activates genes regulating IL-12, IFN-γ, and TNF-α production and adaptive immune responses (Fig. 1D).

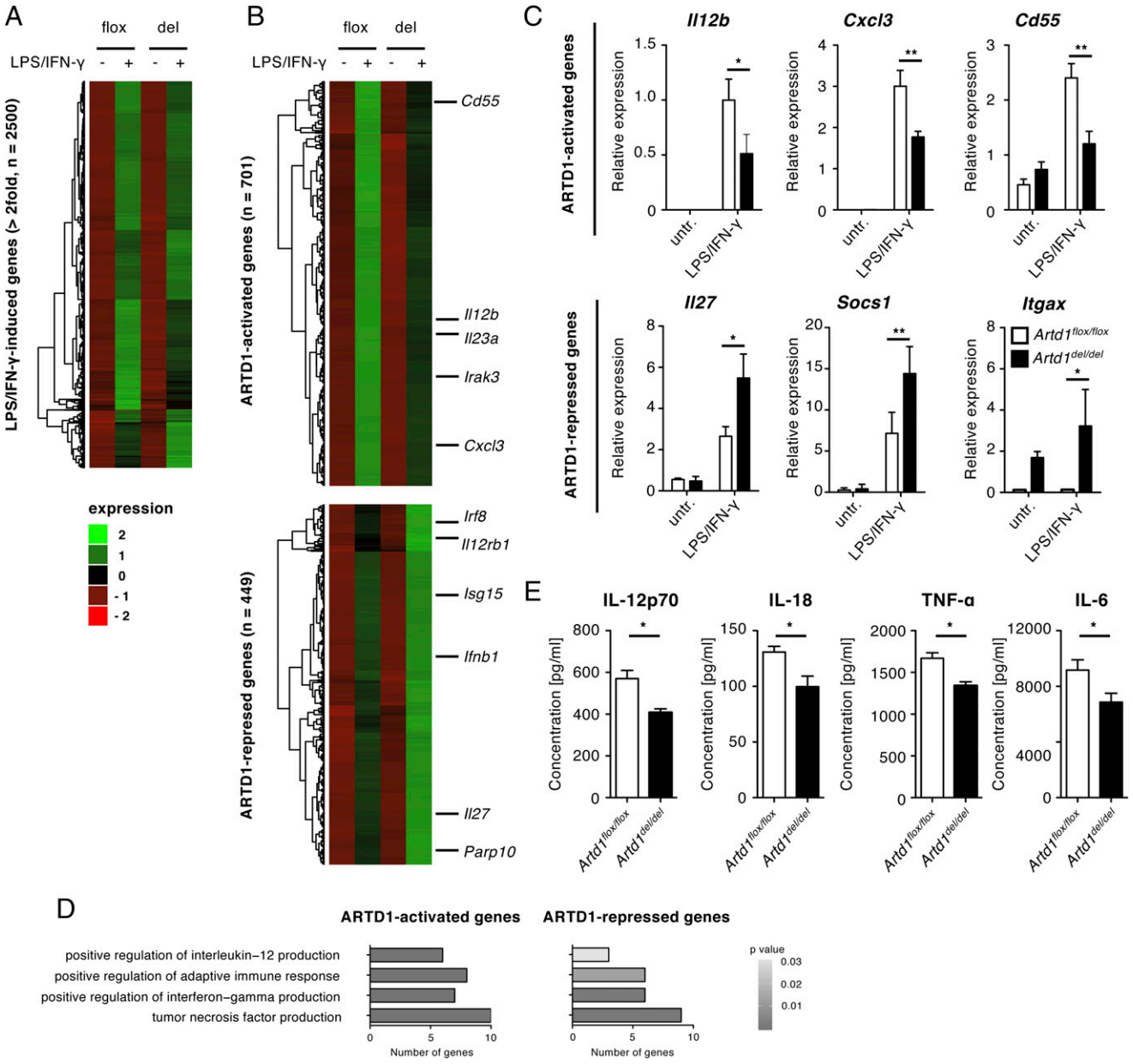

FIGURE 1. ARTD1 regulates proinflammatory gene expression in BMDMs. (**A**) RNA sequencing of total RNA extracted from *Artd1*$^{flox/flox}$ (flox) and *Artd1*$^{del/del}$ (del) BMDMs either left untreated or treated with 10 ng/ml LPS and 2 ng/ml INF-γ for 4 h. The expression levels of all LPS/IFN-γ–induced genes (~2500 genes, fold change ≤2, $p < 0.05$) were clustered. (**B**) Upregulated genes identified in (A) were clustered to identify ARTD1 coactivating (701 genes) and corepressing (449 genes) functions. (**C**) qRT-PCR analysis of selective ARTD1 coactivated and corepressed genes in *Artd1*$^{flox/flox}$ and *Artd1*$^{del/del}$ BMDMs identified in (B). Data are presented as mean ± SD of three biological replicates. (**D**) Gene enrichment analysis of ARTD1 coactivated and ARTD1 corepressed genes [left and right panels, identified in (B)] in *Artd1*$^{flox/flox}$ and *Artd1*$^{del/del}$ BMDMs. (**E**) ELISA of cell culture supernatants for the quantification of the indicated cytokines produced by *Artd1*$^{flox/flox}$ and *Artd1*$^{del/del}$ BMDMs, respectively. Cells were stimulated with 10 ng/ml LPS and 2 ng/ml INF-γ for 18 h. Data are presented as mean concentration ± SD of three independent experiments. *$p < 0.05$, **$p < 0.01$, *t* test.

To investigate whether ARTD1's transcriptional regulation of LPS/IFN-γ–induced target genes depends on its enzymatic activity, the stimulation of BMDMs was repeated in the presence of two ADP-ribosylation inhibitors (i.e., PARPi) (Supplemental Fig. 1H). Although RNA sequencing revealed that treatment of BMDMs with PARPi affected the expression of 267 LPS/IFN-γ–induced genes (Supplemental Fig. 1H), the proinflammatory genes observed above were not affected. Gene ontology analysis of PARPi-sensitive genes revealed no significantly enriched pathways but pH reduction and cell adhesion pathways only in the first cluster ($n = 95$ genes) (Supplemental Fig. 1I). These data suggest that the enzymatic activity of most likely ARTD1 in macrophages does not contribute to LPS/IFN-γ–induced innate immune responses under the examined conditions.

To confirm that the observed transcriptional changes translate into changes at the protein level, the expression levels of differentially regulated cytokines was confirmed by ELISA after treatment of BMDMs cultured from *Artd1*$^{flox/flox}$ and *Artd1*$^{del/del}$ mice for 18 h with LPS/IFN-γ (Fig. 1E). The levels of secreted IL-12p70, IL-18, IL-6, and TNF-α were all significantly reduced in BMDMs from ARTD1-deficient mice compared with wild-type mice. In addition, we analyzed whether the enzymatic activity of ARTD1 regulates proinflammatory cytokine expression at the protein level (Supplemental Fig. 1J). ELISA quantification of

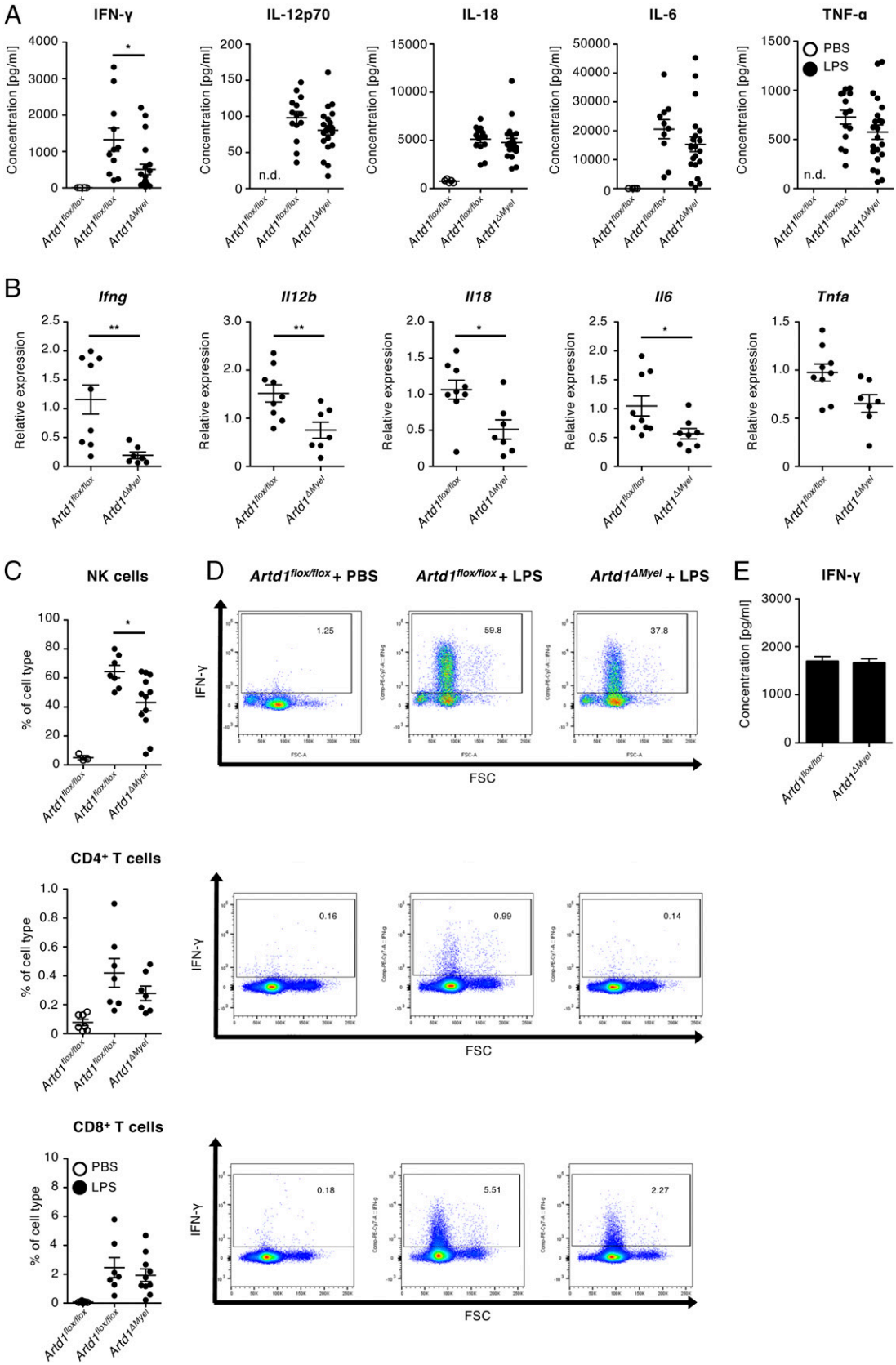

FIGURE 2. Myeloid-specific depletion of ARTD1 reduces the LPS-induced IL-12/18–IFN-γ signaling in vivo. (**A**) *Artd1*$^{flox/flox}$ and *Artd1*$^{\Delta Myel}$ mice were i.p. injected with PBS or 4 mg/kg LPS. After 4 h, whole blood serum was collected, and the selected cytokine levels were quantified by multiplex bead array. Data are shown as mean ± SEM of three independent experiments. (**B**) *Artd1*$^{flox/flox}$ and *Artd1*$^{\Delta Myel}$ mice were i.p. injected with PBS or 4 mg/kg LPS. After 4 h, RNA of total spleen tissue was isolated, and gene expression levels were quantified by qRT-PCR. Data are shown as mean ± SEM of three independent experiments. (**C** and **D**) ICS of splenocytes from *Artd1*$^{flox/flox}$ and *Artd1*$^{\Delta Myel}$ mice i.p. injected with either PBS or 4 mg/kg LPS. After 4 h, intracellular INF-γ was detected by flow cytometry, and the percentages of positively stained NK, CD4$^+$ T, and CD8$^+$ T cells *(Figure legend continues)*

BMDMs stimulated with LPS/IFN-γ in the presence or absence of the PARPi PJ34 or olaparib revealed no expression change for the abovementioned cytokines. These data implicate ARTD1 in the transcriptional control of innate cytokine genes, which is independent of its enzymatic activity and likely to affect type I immune responses in inflammation and cancer models.

Myeloid cell–specific deletion of ARTD1 reduces LPS-induced IL-12/18–IFN-γ signaling in an in vivo model of sterile sepsis

To explore the myeloid cell–intrinsic role of ARTD1 in vivo in models driven by strong T_H1 activation, we crossed the *Artd1*$^{flox/flox}$ mice with transgenic mice harboring a *LyzM-Cre* cassette that resulted in a conditional ARTD1 knockout in lysozyme-expressing myeloid cells (*Artd1*$^{flox/flox}$*;LyzM-cre*), hereafter called *Artd1*$^{\Delta Myel}$ (Supplemental Fig. 2A). Mice lacking ARTD1 specifically in this compartment developed normally and were as fertile as their ARTD1-proficient littermates (data not shown). The correct targeting was confirmed by Western blotting for ARTD1 in vitro in cultured BMDMs and ex vivo in peritoneal macrophages (Supplemental Fig. 2B).

ARTD1-deficient mice are known to be extremely resistant to LPS-induced endotoxic shock (15). We first set out to study the innate immune response to sublethal LPS exposure. To this end, 6–12-wk-old *Artd1*$^{flox/flox}$ and *Artd1*$^{\Delta Myel}$ littermates were i.p. injected with 4 mg/kg body weight of LPS. Both *Artd1*$^{flox/flox}$ and *Artd1*$^{\Delta Myel}$ mice showed the expected clinical symptoms, such as fever and lethargy, but none of the animals died during the 4 h time course of the experiments (data not shown). ELISA-based quantification of serum IFN-γ, IL-12p70, IL-18, TNF-α, and IL-6 levels revealed the strong induction of these cytokines in *Artd1*$^{flox/flox}$ mice upon LPS exposure relative to PBS treatment (Fig. 2A). Interestingly, IFN-γ levels in serum were significantly reduced in *Artd1*$^{\Delta Myel}$ mice, whereas the other tested cytokines were only modestly reduced (Fig. 2A). Analyses of anti-inflammatory or T_H2 cytokines revealed that the serum levels of IL-10 and IL-13 were unchanged, whereas the levels of IL-4 were reduced (Supplemental Fig. 2C), suggesting that the observed differences in proinflammatory cytokine levels were not due to an enhanced anti-inflammatory or T_H2-polarized response. Together, these data confirmed the initiation of an innate immune response with the applied low LPS dose and support the in vitro data that ARTD1-deficient macrophages fail to express IFN-γ–inducing IL-12p70 and IL-18.

The reduced IFN-γ levels in Artd1$^{\Delta Myel}$ *mice are a consequence of the reduced production of IL-12 and IL-18 by macrophages*

Because IL-12 and IL-18 are known to strongly induce IFN-γ gene expression (42), we analyzed the transcript levels of several proinflammatory cytokines in spleen tissue. We found transcript levels of *Ifng*, *Il12b*, *Il18*, *Tnfa*, and *Il6* to be strongly reduced in the spleen of *Artd1*$^{\Delta Myel}$ mice (Fig. 2B), indicating that ARTD1 in macrophages regulates this inflammatory program in vivo. To exclude the possibility that the macrophage-specific deletion of ARTD1 affects the cellular composition of the spleen and thus alters cytokine production, the spleens from *Artd1*$^{flox/flox}$ and *Artd1*$^{\Delta Myel}$ mice were analyzed macroscopically, and their splenocytes were analyzed by flow cytometry using cell type–specific markers. Although the spleen size was not overtly altered (data not shown), the total number of splenocytes was increased in untreated *Artd1*$^{\Delta Myel}$ compared with the *Artd1*$^{flox/flox}$ control mice (Supplemental Fig. 2D). This was fully attributable to an increased number of B and CD4$^+$ T cells, whereas the frequencies of all other examined cell types, including CD8$^+$ T cells, NK cells, and, most importantly, macrophages, monocytes, and neutrophils, were not altered (Supplemental Fig. 2E). These data indicate that the lack of ARTD1 in macrophages neither affected macrophage development nor drastically changed splenic immune cell composition.

IFN-γ is mainly expressed by NK and, to a lesser extent, by T cells during acute inflammation and the onset of an innate immune response (4). To identify the cell type responsible for the reduced IFN-γ levels in the spleen (Fig. 2B), we performed ICS for IFN-γ in NK, CD4$^+$, and CD8$^+$ T cells isolated from the spleens of LPS-treated *Artd1*$^{flox/flox}$ and *Artd1*$^{\Delta Myel}$ mice (Fig. 2C, 2D). Although LPS treatment induced IFN-γ expression in all three analyzed cell types, the frequency of IFN-γ–expressing NK cells was considerably higher than the frequencies of CD4$^+$ and CD8$^+$ T cells. Thus, NK cells appear to be the main source of the differential IFN-γ expression in LPS-treated *Artd1*$^{flox/flox}$ and *Artd1*$^{\Delta Myel}$ mice (Fig. 2C, 2D). To exclude the possibility that NK cells from *Artd1*$^{flox/flox}$ and *Artd1*$^{\Delta Myel}$ mice were differentially responsive to IFN-γ–inducing IL-12/18 signaling, we isolated and stimulated primary NK cells from both genotypes with IL-12p70 (10 ng/ml) for 18 h to quantify their IFN-γ expression by ELISA (Fig. 2E). Stimulation of NK cells from both mouse strains induced IFN-γ expression in an IL-12p70–dependent manner and to the same extent. The combined results indicate that the reduced IFN-γ levels produced by NK cells in *Artd1*$^{\Delta Myel}$ mice exposed to LPS are a consequence of the reduced production of IL-12 and IL-18 by macrophages and that ARTD1 is an important transcriptional activator of these genes.

ARTD1 expression in macrophages is required for T_H1-mediated immune control of bacterial infection

Immunocompetent adult C57BL/6 mice infected with the human gastric pathogen *H. pylori* exhibit a striking T cell infiltration that is dominated by T_H1- and T_H17-polarized CD4$^+$ T cells and limits the bacterial burden (16). We therefore chose this model to assess the role of myeloid ARTD1 expression in anti–*H. pylori* T_H1 responses and infection control. To this end, we first cultured BMDMs from *Artd1*$^{flox/flox}$ and *Artd1*$^{del/del}$ littermates with the human *H. pylori* patient isolate PMSS1 for 6 h. Subsequent qRT-PCR analysis revealed that *H. pylori* robustly induces *Il12b* and *Il1b* gene expression in cultured BMDMs in an, at least in part, ARTD1-dependent manner (Fig. 3A). To investigate the role of ARTD1 expression in myeloid cells for the development of *H. pylori*–specific T_H1 and T_H17 responses in vivo, we infected *Artd1*$^{flox/flox}$ and *Artd1*$^{\Delta Myel}$ mice with 10^8 CFUs of *H. pylori* PMSS1. *Artd1*$^{\Delta Myel}$ mice were colonized at significantly higher levels than their *Artd1*$^{flox/flox}$ counterparts at 4 wk postinfection (Fig. 3B), suggesting that ARTD1 in myeloid cells controls gastric colonization of *H. pylori* in vivo. *H. pylori* induced a strong infiltration of CD4$^+$ T cells into the gastric mucosa that was similar in *Artd1*$^{flox/flox}$ and *Artd1*$^{\Delta Myel}$ mice (Fig. 3C, Supplemental Fig. 3). Interestingly, *H. pylori*–specific T_H1, but not T_H17, responses were dependent on ARTD1 expression in myeloid cells as

were quantified. Data are shown as mean ± SEM of two independent experiments. (**E**) ELISA for IFN-γ secreted from MACS-sorted splenic NK cells that were isolated from *Artd1*$^{flox/flox}$ and *Artd1*$^{\Delta Myel}$ mice. NK cells were stimulated with recombinant murine IL-12p70 (10 ng/ml) for 18 h, and cell culture supernatant was analyzed. $*p < 0.05$, $**p < 0.01$, *t* test.

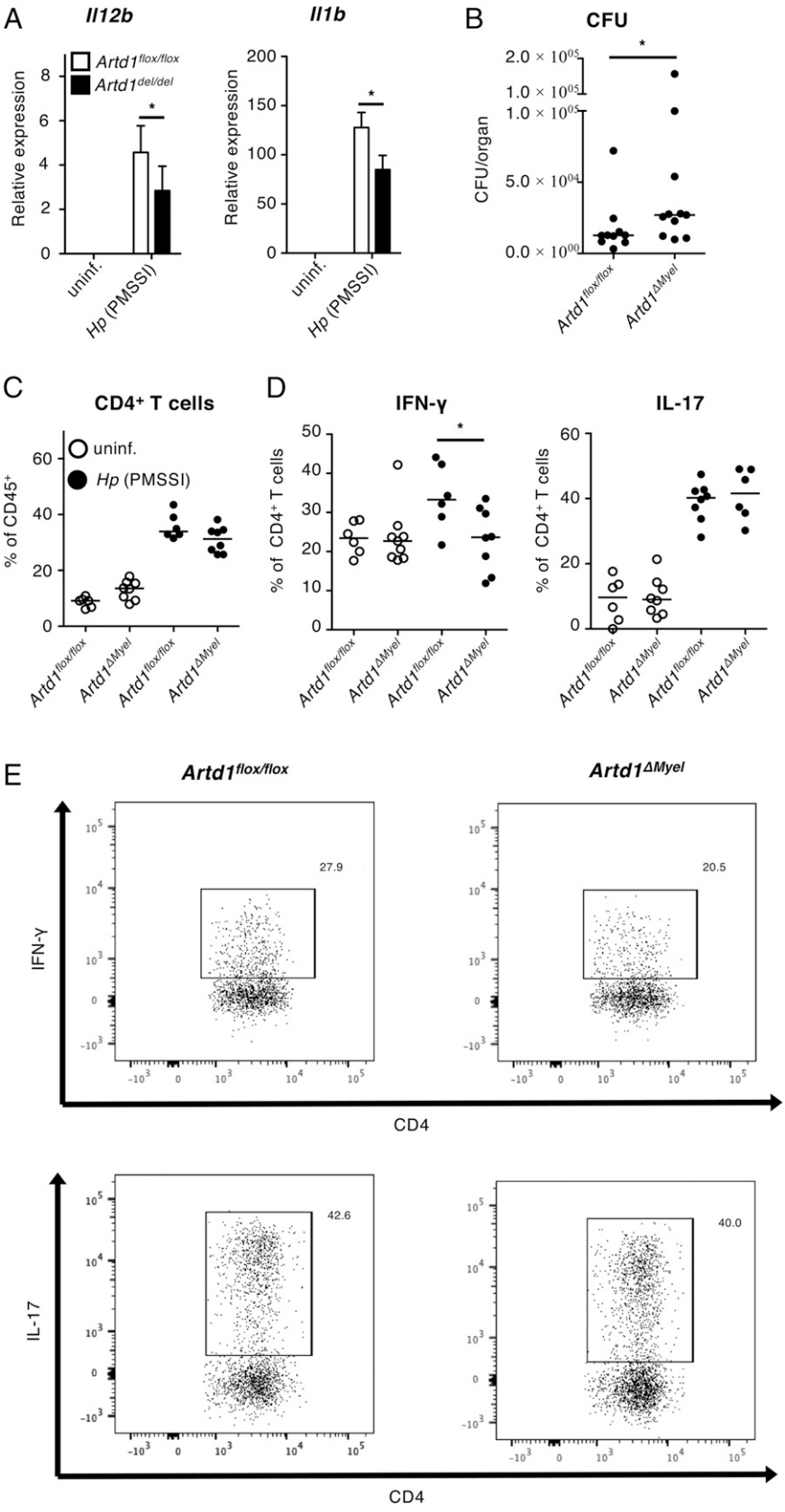

FIGURE 3. ARTD1 in myeloid cells controls *Helicobacter* clearance and anti-*Helicobacter* T_H1 responses. (**A**) qRT-PCR analysis of *Il12b* and *Il1b* expression in *Artd1*$^{flox/flox}$ and *Artd1*$^{del/del}$ BMDMs. Cells were either left untreated or incubated with *H. pylori* (multiplicity of infection 50) for 6 h. Data are presented as median ± SEM of three technical replicates; one representative experiment of two is shown. (**B**–**E**) Mice of the indicated genotypes were orally infected with *H. pylori*. Gastric colonization as assessed by plating and colony counting is shown in (B). Gastric $CD4^+$ T cell infiltration and IFN-γ and IL-17 expression by $CD4^+$ T cells, as determined by ICS, are shown in (C) and (D). Horizontal lines in (B)–(D) indicate medians. Representative FACS plots are presented in (E). Data in (B) are pooled from two independent studies; data in (C) and (D) are from one representative study of two independently conducted ones. $*p < 0.05$, $**p < 0.01$, *t* test.

assessed by intracellular staining for the signature cytokines IFN-γ and IL-17 (Fig. 3D, 3E). The combined results suggest that ARTD1 expression in myeloid cells is specifically required for IL-12–driven T_H1 polarization and infection control but not for T_H17 responses or $CD4^+$ T cell recruitment.

Expression of ARTD1 in myeloid cells controls the T cell–mediated immune control of MC-38 tumors

Understanding the impact of myeloid cells on cancer development is essential in distinguishing and possibly manipulating positive and negative myeloid effectors. Polarization states of intratumoral

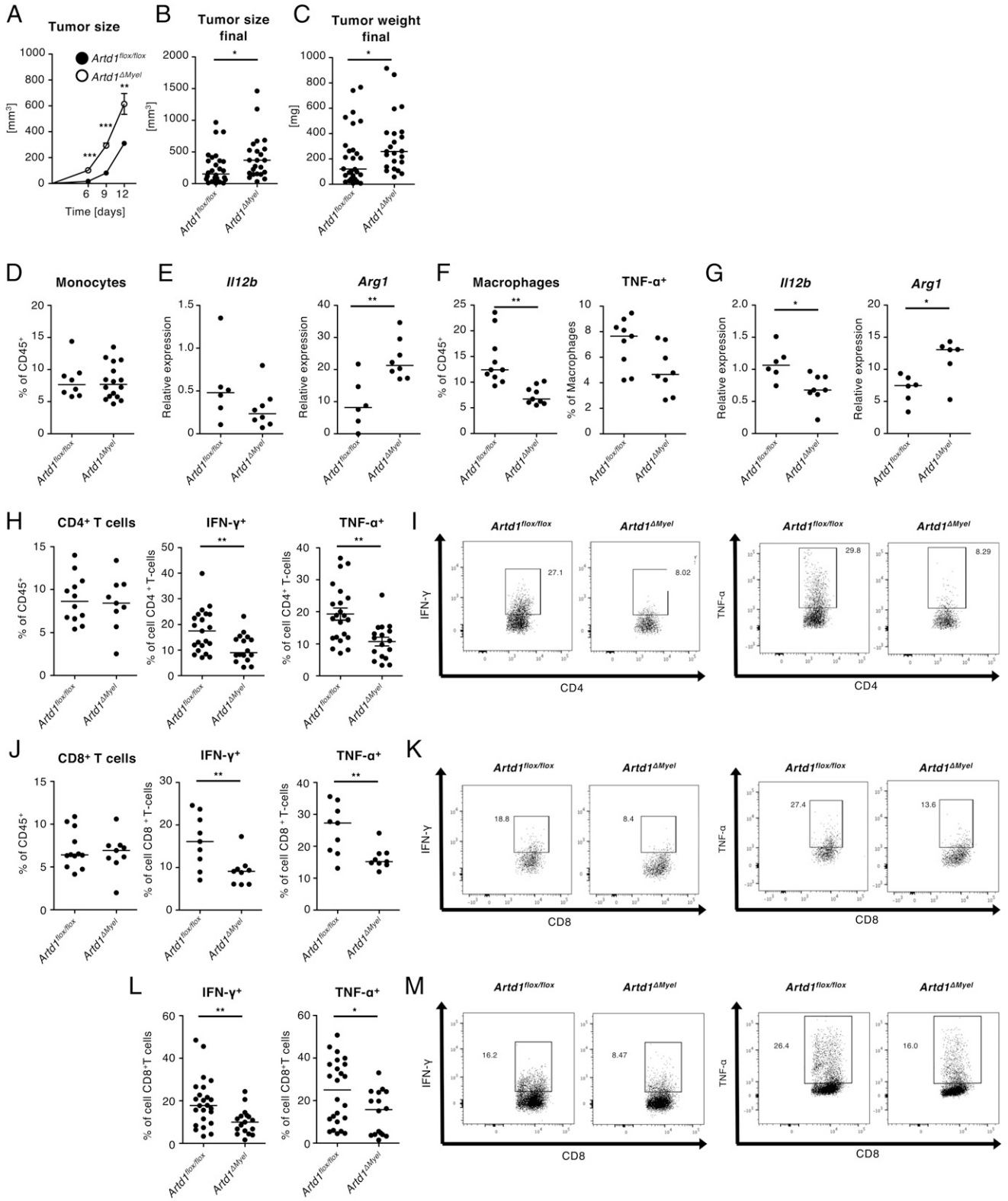

FIGURE 4. ARTD1 controls macrophage infiltration and CD4$^+$/CD8$^+$ T cell activation in MC-38 tumors. (**A**–**C**) Tumor volume and weight of MC-38 tumors s.c. injected into the flanks of *Artd1*$^{flox/flox}$ and *Artd1*$^{\Delta Myel}$ mice, as determined by caliper measurements at the indicated time points and at the study's end point. Each symbol represents one mouse. Data are pooled from two independent experiments and presented as mean ± SEM (A). Horizontal lines in (B) and (C) indicate medians. (**D**) Monocyte infiltration of of MC-38 tumors grown on the flanks of *Artd1*$^{flox/flox}$ and *Artd1*$^{\Delta Myel}$ mice, as quantified by flow cytometry. (**E**) *Il12b* and *Arg1* expression of FACS-sorted tumor-infiltrating monocytes, as determined by qRT-PCR. Data in (E) are from one representative experiment of two; horizontal lines indicate medians. (**F**) Total and TNF-α$^+$ tumor-infiltrating macrophages, as quantified by flow cytometry. (**G**) *Il12b* and *Arg1* expression of FACS-sorted tumor-infiltrating macrophages, as determined by qRT-PCR. Data are from one representative experiment of two; horizontal lines indicate medians. (**H** and **I**) Infiltration and IFN-γ and TNF-α expression of CD4$^+$ T cells, as flow cytometrically determined after ex vivo restimulation with PMA/ionomycin. Data are from one representative experiment (left panel) or pooled from two independent experiments (right panels). Representative FACS plots are shown in (I). (**J** and **K**) Infiltration and IFN-γ and TNF-α expression of *(Figure legend continues)*

myeloid populations contribute differentially to tumorigenesis (25). Tumor-associated macrophages infiltrate tumors and can serve as important initiators of T_H1-mediated antitumor immunity in some settings but have also been described as promoting tumor growth in others (43). To investigate a possible myeloid-specific ARTD1 contribution to antitumor immunity, we injected 0.5×10^6 MC-38 colon adenocarcinoma cells s.c. into the flanks of *Artd1*$^{flox/flox}$ and *Artd1*$^{\Delta Myel}$ mice. *Artd1*$^{\Delta Myel}$ mice sustained a significantly increased tumor burden from day 6 onwards relative to their *Artd1*$^{flox/flox}$ littermates, which was evident until the study's end point (Fig. 4A–C). Ly6C$^+$ MHC class II$^+$ monocytes, identified according to the gating strategy shown in Supplemental Fig. 4, infiltrated the tumors at a similar rate irrespective of ARTD1 status but expressed less *Il12b* and more *Arg1* as judged by qRT-PCR of FACS-sorted cells if lacking ARTD1 (Fig. 4D, 4E). F4/80$^+$ macrophage frequencies in the tumor microenvironment were decreased in *Artd1*$^{\Delta Myel}$ mice (Fig. 4F), and fewer macrophages expressed TNF-α (Fig. 4F) and *Il12b* (Fig. 4G) as judged by intracellular staining and qRT-PCR of sorted cells, respectively. As observed for monocytes, *Arg1* gene expression was enhanced in macrophages as a consequence of ARTD1 deficiency (Fig. 4G). The data suggest that ARTD1 potentially affects the differentiation of macrophages from inflammatory monocytes as well as their M1 polarization. Interestingly, the loss of ARTD1 in myeloid cells further resulted in strongly reduced intratumoral CD4$^+$ and CD8$^+$ T cell activation as judged by IFN-γ– and TNF-α–specific staining, although the recruitment of both populations to the tumor microenvironment was unaffected (Fig. 4H–K). The differences due to ARTD1 deficiency in CD8$^+$ T cell activation could be confirmed by restimulation with MC-38 tumor-specific peptide (Fig. 4L, 4M)

The combined results implicate myeloid-intrinsic ARTD1 expression in the generation and/or maintenance of type I immunity in models of LPS challenge, bacterial infection, and tumor growth.

Discussion

In this study, we investigated the role of ARTD1 in models of myeloid cell activation in response to innate immune stimulation, bacterial infection, and MC-38 tumor growth. We show that ARTD1 expression in myeloid cells controls a transcriptional program that includes T_H1-polarizing cytokines and type I immunity; this function of ARTD1 appears to be independent of its ADP-ribosylating activity, as inhibitors targeting the enzymatic function of ARTD1 do not recapitulate the effects of loss of the protein.

Various reports have shown that ARTD1 acts as a transcriptional cofactor for NF-κB and promotes gene expression by functional cooperation with the transcription machinery in response to proinflammatory stimuli (44). LPS- and TNF-α–induced NF-κB–dependent gene expression in macrophages and fibroblasts was enhanced by ARTD1 independently of its enzymatic activity through the initiation of a mediator complex that also contains p300 and NF-κB. In the current study, treatment of BMDMs with ADP-ribosylation inhibitors (e.g., olaparib or PJ34) did not affect the expression of LPS/IFN-γ–induced gene expression, although some non–inflammation-related genes involved in pH reduction and cell adhesion were susceptible to both inhibitors. In contrast, another report suggested that LPS treatment of macrophages induced ARTD1's enzymatic activity and nucleosome remodeling at promoters of proinflammatory genes, which directly destabilized histone–DNA interactions and facilitated NF-κB binding and gene expression (45). The discrepancies could be explained by methodological differences, such as the cell type (RAW267.4 macrophages and primary BMDMs or fibroblasts), the source of LPS (*Salmonella enterica* and *E. coli*), or the serum starvation overnight prior to LPS stimulation.

The LPS-induced expression of IL-12/18 in primary macrophages was strongly dependent on ARTD1 ex vivo as well as in vivo. The *Il12b* gene is a well studied example of a gene that requires chromatin remodeling during inflammation-induced gene expression (46). Studies of the *Il12b* promoter identified binding sites for various transcription factors including NF-κB, C/EBP, AP-1, and NFAT (42). However, their binding sites, 30–175 bp upstream of the transcription start site, are blocked by nucleosomes and require nucleosome remodeling prior to transcription (46). Indeed, the SWI-SNF complex that is responsible for nucleosome positioning is recruited to target genes in LPS-stimulated macrophages (47). Several models describe the targeting of chromatin remodeling machines to their site of action (i.e., acetylated histones that target and stabilize the SWI-SNF complex at target loci) (48). Very recently, another report confirmed that small hairpin RNA–mediated knockdown of endogenous ARTD1 expression resulted in reduced *Il12b* mRNA expression and *Il12b* promoter activity (49). BMDMs from ARTD1-deficient mice also exhibited decreased IL-12p40 expression at both mRNA and protein levels.

IL-12 connects innate and adaptive immune responses either indirectly via NK cell activation or directly by activating CD4$^+$ and CD8$^+$ T cells (5). In this study, we observed a reduced NK cell activation after LPS administration in *Artd1*$^{\Delta Myel}$ compared with *Artd1*$^{flox/flox}$ mice. Our analyses of the splenic cell composition of *Artd*$^{\Delta Myel}$ relative to *Artd1*$^{flox/flox}$ mice revealed that, whereas B and CD4$^+$ T cell counts were increased, all other analyzed cell types, including monocytes and macrophages, were not altered, suggesting that the deletion of ARTD1 in myeloid cells did not decrease the numbers of other cell types and their functionality in this organ. ARTD1-deficient macrophages (or other myeloid cells) failed to activate NK cells via IL-12 expression, ultimately leading to decreased IFN-γ serum levels and thus protecting against the consequences of LPS administration. Several lines of evidence suggest that NK cells might be involved in key functions during sepsis (4). Similar to the observations made in ARTD1-deficient mice, Ab-mediated NK cell depletion in vivo protected against LPS-induced shock and significantly decreased IFN-γ cytokine levels (15) During sepsis, NK cells promote and amplify the inflammatory response as a very early and main source of IFN-γ, and thus represent a promising target for novel approaches in sepsis therapy (4).

Reduced NK cell activation significantly reduces the kinetics of pathogen clearance during sepsis (4). Thus, by enhancing *Il12b* expression in myeloid cells, ARTD1 contributes to the generation of a potent immune response to pathogens. This was very obvious in the second disease model we investigated. Previous studies characterized the stomach under basal conditions to be a predominantly myeloid cell–controlled organ with little or no lymphocyte immune surveillance (29). Myeloid cells centrally

CD8$^+$ T cells, as flow cytometrically determined after ex vivo restimulation with PMA/ionomycin. Data in (J) are from one representative experiment of two. (**L** and **M**) Infiltration and IFN-γ and TNF-α expression of CD8$^+$ T cells, as flow cytometrically determined after ex vivo restimulation with MC-38–specific peptide. Data are pooled from two experiments; horizontal lines indicate medians throughout. *$p < 0.05$, **$p < 0.01$, *t* test.

function as initiators of immune responses against pathogens. Our study revealed that ARTD1 deficiency does not affect gastric $CD4^+$ T cell recruitment during *H. pylori* infection but that the loss of ARTD1 results in reduced T_H1 frequencies. Thus, ARTD1 drives pathogen control via IL-12 production and the initiation of potent immune responses.

Macrophages play important yet bimodal roles in orchestrating tumor-associated immune responses (43). They are involved in tumor killing and other effector functions, but they can also promote tumor growth by skewing and suppressing T cell responses. We made several observations relating to ARTD1 of macrophages in the MC-38 tumor model. On the one hand, we find fewer macrophages in the tumor microenvironment of *Artd1*$^{\Delta Myel}$ mice, whereas monocyte frequencies are unchanged, which indicates that macrophage differentiation is impaired in the absence of ARTD1 expression. On the other hand, those macrophages that do infiltrate the tumors (or differentiate there from their monocyte precursors) express less TNF-α and less IL-12 but more Arginase 1, indicating that they have adopted an M2-polarized state. As a consequence of their lower intratumoral macrophage frequencies, combined with their dysregulated macrophage activation and polarization, *Artd1*$^{\Delta Myel}$ mice fail to generate appropriate T_H1-polarized $CD4^+$ and cytotoxic $CD8^+$ T cell responses and therefore cannot control the tumor burden as efficiently as wild-type littermates.

Taken together, the results of this study identify ARTD1 expression in myeloid cell types as a critical regulator of proinflammatory IL-12/18 cytokine expression. In particular, ARTD1 controls the initiation of potent immune responses to LPS and the elimination of pathogens and tumors in vivo.

Acknowledgments

We thank Tobias Suter (University of Zurich) for helpful discussions and for providing editorial assistance. We thank Maria Domenica Moccia and Giancarlo Russo from the Functional Genomics Center of the University of Zurich for RNA sequencing and data analysis. We also thank Raffaella Santoro (University of Zurich) for providing the CMV-Cre mouse strain.

Disclosures

The authors have no financial conflicts of interest.

References

1. Iwasaki, A., and R. Medzhitov. 2015. Control of adaptive immunity by the innate immune system. *Nat. Immunol.* 16: 343–353.
2. Antoine, R., and C. Locht. 1990. Roles of the disulfide bond and the carboxy-terminal region of the S1 subunit in the assembly and biosynthesis of pertussis toxin. *Infect. Immun.* 58: 1518–1526.
3. Simon, N. C., K. Aktories, and J. T. Barbieri. 2014. Novel bacterial ADP-ribosylating toxins: structure and function. *Nat. Rev. Microbiol.* 12: 599–611.
4. Chiche, L., J.-M. Forel, G. Thomas, C. Farnarier, F. Vely, M. Bléry, L. Papazian, and E. Vivier. 2011. The role of natural killer cells in sepsis. *J. Biomed. Biotechnol.* 2011: 986491.
5. Chaudhry, H., J. Zhou, Y. Zhong, M. M. Ali, F. McGuire, P. S. Nagarkatti, and M. Nagarkatti. 2013. Role of cytokines as a double-edged sword in sepsis. *In Vivo* 27: 669–684.
6. Ramirez-Carrozzi, V. R., A. A. Nazarian, C. C. Li, S. L. Gore, R. Sridharan, A. N. Imbalzano, and S. T. Smale. 2006. Selective and antagonistic functions of SWI/SNF and Mi-2beta nucleosome remodeling complexes during an inflammatory response. *Genes Dev.* 20: 282–296.
7. Hassa, P. O., S. S. Haenni, M. Elser, and M. O. Hottiger. 2006. Nuclear ADP-ribosylation reactions in mammalian cells: where are we today and where are we going? *Microbiol. Mol. Biol. Rev.* 70: 789–829.
8. Bai, P., and L. Virág. 2012. Role of poly(ADP-ribose) polymerases in the regulation of inflammatory processes. *FEBS Lett.* 586: 3771–3777.
9. Ba, X., and N. J. Garg. 2011. Signaling mechanism of poly(ADP-ribose) polymerase-1 (PARP-1) in inflammatory diseases. *Am. J. Pathol.* 178: 946–955.
10. Hottiger, M. O., P. O. Hassa, B. Lüscher, H. Schüler, and F. Koch-Nolte. 2010. Toward a unified nomenclature for mammalian ADP-ribosyltransferases. *Trends Biochem. Sci.* 35: 208–219.
11. Gupte, R., Z. Liu, and W. L. Kraus. 2017. PARPs and ADP-ribosylation: recent advances linking molecular functions to biological outcomes. *Genes Dev.* 31: 101–126.
12. Ray Chaudhuri, A., and A. Nussenzweig. 2017. The multifaceted roles of PARP1 in DNA repair and chromatin remodelling. *Nat. Rev. Mol. Cell Biol.* 18: 610–621.
13. Lord, C. J., and A. Ashworth. 2017. PARP inhibitors: synthetic lethality in the clinic. *Science* 355: 1152–1158.
14. Berger, N. A., V. C. Besson, A. H. Boulares, A. Bürkle, A. Chiarugi, R. S. Clark, N. J. Curtin, S. Cuzzocrea, T. M. Dawson, V. L. Dawson, et al. 2018. Opportunities for the repurposing of PARP inhibitors for the therapy of non-oncological diseases. *Br. J. Pharmacol.* 175: 192–222.
15. Oliver, F. J., J. Ménissier-de Murcia, C. Nacci, P. Decker, R. Andriantsitohaina, S. Muller, G. de la Rubia, J. C. Stoclet, and G. de Murcia. 1999. Resistance to endotoxic shock as a consequence of defective NF-kappaB activation in poly (ADP-ribose) polymerase-1 deficient mice. *EMBO J.* 18: 4446–4454.
16. Koch, K. N., and A. Müller. 2015. *Helicobacter pylori* activates the TLR2/NLRP3/caspase-1/IL-18 axis to induce regulatory T-cells, establish persistent infection and promote tolerance to allergens. *Gut Microbes* 6: 382–387.
17. Arnold, I. C., J. Y. Lee, M. R. Amieva, A. Roers, R. A. Flavell, T. Sparwasser, and A. Müller. 2011. Tolerance rather than immunity protects from *Helicobacter pylori*-induced gastric preneoplasia. *Gastroenterology* 140: 199–209.
18. Harris, P. R., S. W. Wright, C. Serrano, F. Riera, I. Duarte, J. Torres, A. Peña, A. Rollán, P. Viviani, E. Guiraldes, et al. 2008. *Helicobacter pylori* gastritis in children is associated with a regulatory T-cell response. *Gastroenterology* 134: 491–499.
19. Toller, I. M., M. Altmeyer, E. Kohler, M. O. Hottiger, and A. Müller. 2010. Inhibition of ADP ribosylation prevents and cures *helicobacter*-induced gastric preneoplasia. *Cancer Res.* 70: 5912–5922.
20. Hassa, P. O., and M. O. Hottiger. 1999. A role of poly (ADP-ribose) polymerase in NF-kappaB transcriptional activation. *Biol. Chem.* 380: 953–959.
21. Hassa, P. O., M. Covic, S. Hasan, R. Imhof, and M. O. Hottiger. 2001. The enzymatic and DNA binding activity of PARP-1 are not required for NF-kappa B coactivator function. *J. Biol. Chem.* 276: 45588–45597.
22. Hassa, P. O., S. S. Haenni, C. Buerki, N. I. Meier, W. S. Lane, H. Owen, M. Gersbach, R. Imhof, and M. O. Hottiger. 2005. Acetylation of poly(ADP-ribose) polymerase-1 by p300/CREB-binding protein regulates coactivation of NF-kappaB-dependent transcription. *J. Biol. Chem.* 280: 40450–40464.
23. Piccard, H., R. J. Muschel, and G. Opdenakker. 2012. On the dual roles and polarized phenotypes of neutrophils in tumor development and progression. *Crit. Rev. Oncol. Hematol.* 82: 296–309.
24. Souto, J. C., L. Vila, and A. Brú. 2011. Polymorphonuclear neutrophils and cancer: intense and sustained neutrophilia as a treatment against solid tumors. *Med. Res. Rev.* 31: 311–363.
25. Gabrilovich, D. I., S. Ostrand-Rosenberg, and V. Bronte. 2012. Coordinated regulation of myeloid cells by tumours. *Nat. Rev. Immunol.* 12: 253–268.
26. Roblek, M., M. Calin, M. Schlesinger, D. Stan, R. Zeisig, M. Simionescu, G. Bendas, and L. Borsig. 2015. Targeted delivery of CCR2 antagonist to activated pulmonary endothelium prevents metastasis. *J. Control. Release* 220(Pt A): 341–347.
27. Müller-Edenborn, K., K. Léger, J. F. Glaus Garzon, C. Oertli, A. Mirsaidi, P. J. Richards, H. Rehrauer, P. Spielmann, D. Hoogewijs, L. Borsig, et al. 2015. Hypoxia attenuates the proinflammatory response in colon cancer cells by regulating IκB. *Oncotarget* 6: 20288–20301.
28. Skarnes, W. C., B. Rosen, A. P. West, M. Koutsourakis, W. Bushell, V. Iyer, A. O. Mujica, M. Thomas, J. Harrow, T. Cox, et al. 2011. A conditional knockout resource for the genome-wide study of mouse gene function. *Nature* 474: 337–342.
29. Arnold, I. C., X. Zhang, S. Urban, M. Artola-Borán, M. G. Manz, K. M. Ottemann, and A. Müller. 2017. NLRP3 controls the development of gastrointestinal $CD11b^+$ dendritic cells in the steady state and during chronic bacterial infection. *Cell Rep.* 21: 3860–3872.
30. Lim, S. Y., A. E. Yuzhalin, A. N. Gordon-Weeks, and R. J. Muschel. 2016. Tumor-infiltrating monocytes/macrophages promote tumor invasion and migration by upregulating S100A8 and S100A9 expression in cancer cells. *Oncogene* 35: 5735–5745.
31. Zhang, X., R. Goncalves, and D. M. Mosser. 2008. The isolation and characterization of murine macrophages. *Curr. Protoc. Immunol.* Chapter 14: Unit 14.1.
32. Fortier, A. H., and L. A. Falk. 2001. Isolation of murine macrophages. *Curr. Protoc. Immunol.* Chapter 14: Unit 14.1–14.1.9.
33. Spath, S., J. Komuczki, M. Hermann, P. Pelczar, F. Mair, B. Schreiner, and B. Becher. 2017. Dysregulation of the cytokine GM-CSF induces spontaneous phagocyte invasion and immunopathology in the central nervous system. *Immunity* 46: 245–260.
34. Bolger, A. M., M. Lohse, and B. Usadel. 2014. Trimmomatic: a flexible trimmer for Illumina sequence data. *Bioinformatics* 30: 2114–2120.
35. Dobin, A., C. A. Davis, F. Schlesinger, J. Drenkow, C. Zaleski, S. Jha, P. Batut, M. Chaisson, and T. R. Gingeras. 2013. STAR: ultrafast universal RNA-seq aligner. *Bioinformatics* 29: 15–21.
36. Lawrence, M., W. Huber, H. Pagès, P. Aboyoun, M. Carlson, R. Gentleman, M. T. Morgan, and V. J. Carey. 2013. Software for computing and annotating genomic ranges. *PLoS Comput. Biol.* 9: e1003118.
37. Robinson, M. D., D. J. McCarthy, and G. K. Smyth. 2010. edgeR: a Bioconductor package for differential expression analysis of digital gene expression data. *Bioinformatics* 26: 139–140.
38. Minotti, R., A. Andersson, and M. O. Hottiger. 2015. ARTD1 suppresses interleukin 6 expression by repressing MLL1-dependent histone H3 trimethylation. *Mol. Cell. Biol.* 35: 3189–3199.

39. Abplanalp, J., M. Leutert, E. Frugier, K. Nowak, R. Feurer, J. Kato, H. V. A. Kistemaker, D. V. Filippov, J. Moss, A. Caflisch, and M. O. Hottiger. 2017. Proteomic analyses identify ARH3 as a serine mono-ADP-ribosylhydrolase. *Nat. Commun.* 8: 2055.
40. Bürkle, A., and L. Virág. 2013. Poly(ADP-ribose): PARadigms and PARadoxes. *Mol. Aspects Med.* 34: 1046–1065.
41. Wang, Z. Q., B. Auer, L. Stingl, H. Berghammer, D. Haidacher, M. Schweiger, and E. F. Wagner. 1995. Mice lacking ADPRT and poly(ADP-ribosyl)ation develop normally but are susceptible to skin disease. *Genes Dev.* 9: 509–520.
42. Ma, X., W. Yan, H. Zheng, Q. Du, L. Zhang, Y. Ban, N. Li, and F. Wei. 2015. Regulation of IL-10 and IL-12 production and function in macrophages and dendritic cells. *F1000 Res.* 4: 1465.
43. Mantovani, A., F. Marchesi, A. Malesci, L. Laghi, and P. Allavena. 2017. Tumour-associated macrophages as treatment targets in oncology. *Nat. Rev. Clin. Oncol.* 14: 399–416.
44. Krishnakumar, R., and W. L. Kraus. 2010. The PARP side of the nucleus: molecular actions, physiological outcomes, and clinical targets. *Mol. Cell* 39: 8–24.
45. Hassa, P. O., and M. O. Hottiger. 2002. The functional role of poly(ADP-ribose) polymerase 1 as novel coactivator of NF-kappaB in inflammatory disorders. *Cell. Mol. Life Sci.* 59: 1534–1553.
46. Weinmann, A. S., D. M. Mitchell, S. Sanjabi, M. N. Bradley, A. Hoffmann, H. C. Liou, and S. T. Smale. 2001. Nucleosome remodeling at the IL-12 p40 promoter is a TLR-dependent, Rel-independent event. *Nat. Immunol.* 2: 51–57.
47. Lai, D., M. Wan, J. Wu, P. Preston-Hurlburt, R. Kushwaha, T. Grundström, A. N. Imbalzano, and T. Chi. 2009. Induction of TLR4-target genes entails calcium/calmodulin-dependent regulation of chromatin remodeling. *Proc. Natl. Acad. Sci. USA* 106: 1169–1174.
48. Becker, P. B., and W. Hörz. 2002. ATP-dependent nucleosome remodeling. *Annu. Rev. Biochem.* 71: 247–273.
49. Zhao, Q., Q. Du, F. Wei, J. Xie, and X. Ma. 2017. An infectious disease-associated *Il12b* polymorphism regulates IL-12/23 p40 transcription involving poly(ADP-ribose) polymerase 1. *J. Immunol.* 198: 2935–2942.